ELSEVIER

Earth and Planetary Science Letters 199 (2002) 157–172

EPSL

www.elsevier.com/locate/epsl

Heterogeneous heat production in the Earth's upper mantle: blob melting and MORB composition

I. Vlastélic [a,b,*], H. Bougault [a], L. Dosso [c]

[a] *IFREMER, B.P. 70, 29280 Plouzané, France*
[b] *Max-Planck-Institut für Chemie, Postfach 3060, 55020 Mainz, Germany*
[c] *UMR 6538, IFREMER, B.P. 70, 29280 Plouzané, France*

Received 10 August 2001; received in revised form 5 February 2002; accepted 14 February 2002

Abstract

The existence of heat-producing elements (U, Th, K) and their highly heterogeneous distribution in the Earth's mantle suggests a link between thermal and chemical properties of the mantle. Previous studies have shown that this chemical–thermal relationship has a strong influence on the mantle convection pattern and structure. Here, we investigate the influence of this relationship on mantle melting and chemical variations in mid-ocean ridge basalts (MORB). We use a model of convection in which mantle heterogeneities are considered as enriched blobs (enrichment factor of $\sim$1.8 relative to the bulk silicate Earth) within a convecting depleted medium.

Our results explain the first-order chemical variations in MORB in terms of coupled compositional–thermal variations in the underlying mantle source. A consequence is that enriched MORB are formed by larger partial melting extent than depleted MORB. We show that: (1) excess temperatures of up to 100°C are produced in the centers of large (300 km radius) and enriched blobs, and these lead to a 10% increase in the degree of melting. Such large blobs could produce long-wavelength chemical anomalies in MORB whose amplitude, however, is attenuated by extensive melting. Small blobs (radius <100 km), in which only minor temperature excesses ($\Delta T<10$°C) develop, may be the cause of high-amplitude chemical spikes along spreading ridges. (2) The maximum temperature gradient within blobs is lower than the solidus slope, which causes the blob to melt progressively from top to bottom. (3) Source enrichment and the degree of melting are positively correlated but the two parameters have competing effects on MORB composition. Normally the source effect is more important than the melting effect. (4) Melting of homogeneous blobs results in a U-shaped chemical anomaly in MORB, the less enriched liquids corresponding to the maximum thermal anomaly. Blobs containing a chemical gradient, with the more depleted composition towards the periphery, may result from entrainment of surrounding depleted mantle. Such blobs, which are thermally more stable, could produce the hump-shaped chemical anomalies commonly observed along mid-ocean ridges.

Keywords: upper mantle; heat sources; melting; mid-ocean ridge basalts

1. Introduction

The slow radioactive decay of uranium, thorium and potassium provides a major, continuous

* Corresponding author. Present address: UMR 5025, LGCA, B.P. 53, 38041 Grenoble Cedex 9, France. Tel.: +33-4-76-63-59-08.
E-mail address: ivlastel@ujf-grenoble.fr (I. Vlastélic).

0012-821X/02/$ – see front matter
PII: S0012-821X(02)00538-1

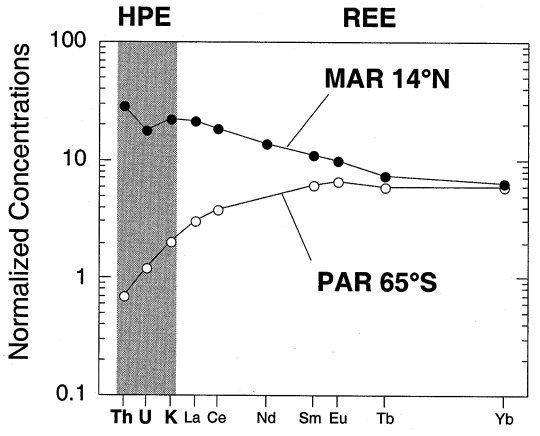

Fig. 1. Extended rare earth element plot. Rare earth elements (REE) provide the main sequence of incompatibility to which heat-producing elements (HPE) are compared. Since heat-producing elements variations in MORB are larger than those shown by the lightest rare earth elements (La and Ce), heat-producing elements plot at the left end of the sequence indicating that they belong to the most incompatible elements. The enriched and depleted patterns are from the Mid-Atlantic Ridge at 14°N (sample 2ΠD43lv) and the Pacific-Antarctic Ridge at 64°S (sample CV04v), respectively ([47–49]; and unpublished data). All concentrations are normalized to primitive mantle values given in [29].

source of heat within the Earth. The distribution in the mantle of these heat-producing elements has been used to constrain the thermal [1–6] and degassing [7] history of the Earth, and the geometry of mantle convection [8]. These elements have another important property whose consequences have, surprisingly, received less attention. They are highly incompatible (they have a strong affinity for liquids) and this causes them to be concentrated in magmas and depleted in the residues of melting. Their concentrations in the mantle probably are highly variable and this variation may contribute to mantle convection [9]. Recent thermo-chemical models [10–12] have taken into account the influence on convection patterns of a highly variable distribution of the heat-producing elements, and the movement of these heat sources, providing a more realistic view of mantle dynamics and evolution. These models suggest that chemical heterogeneity can be preserved for geologically long times even during whole-mantle convection. It has also been shown [13] that melt extraction can generate considerable heterogeneity in the distribution of these elements. A fundamental issue emphasized by Ogawa [13] is that coupling between magmatism and convection should strongly influence the thermal and chemical structure of the mantle.

This paper focuses on melting of a mantle with highly variable distribution of the heat-producing elements. It is based on the observation that these elements are highly incompatible [14–17] and, as a consequence, display the largest variations of concentration in mid-ocean ridge basalts (MORB) (Fig. 1). As illustrated by the selected values given in Table 1, these concentrations vary by at least a factor of 10. Since MORB are probably produced by relatively large degrees of melting ($>8\%$) [18–21], large variations in the concentrations of heat-producing elements are also expected in the underlying mantle source. This heterogeneity should have a strong influence on mantle temperatures and hence on the degrees of melting: domains enriched in heat-producing elements are expected to be hotter, and they will intersect the solidus at greater depth and melt more than depleted domains. Therefore, the extent of mantle enrichment and of partial melting should be positively correlated. On the other hand, the two processes should have opposing effects on MORB compositions. By linking mantle temperatures to the concentrations of heat-producing elements, we should be able to evaluate the relative importance of these competing effects on MORB compositions.

Heat-producing elements should also play a significant role in determining the temperatures of mantle plumes, which should be strongly enriched in highly incompatible elements. Indeed, it has been suggested that high concentrations of heat-producing elements could result in a more rapid growth of plumes [10]. The present study, however, is restricted to the MORB source because of the complexity of the melting that generates ocean island basalts. The simple assumptions used in this study (a constant final depth of melting or no lithosphere contamination) are valid, at first approximation, for MORB generation but clearly do not hold for the generation of ocean island basalts. In contrast with previous studies, this pa-

per considers both enriched and depleted MORB. Enriched MORB are explained by the presence of enriched domains in the upper mantle; the origin of these domains and their relationship with near-ridge hotspots is not the object of this paper.

The relationship between composition and temperature is not straightforward because the temperature of a mantle domain depends not only on the concentration of heat-producing elements, but also on the size of the domain, its geometry, and the mode of heat loss. In this study, we model mantle domains as blobs. This is both realistic and convenient; realistic because blobs may persist for billions of years in the convective mantle [22,23], convenient because diffusive heat transfer can be simply treated. We use the blob model of convection as proposed by Becker et al. [24]: the blobs are treated as non-deformable domains with steady-state heat diffusion and their time evolution is ignored. We show that these assumptions are reasonable and develop the blob model to investigate the consequences of variable concentrations of heat-producing elements in the upper mantle. We focus in particular on the consequences of blob melting on MORB compositions, and suggest that the first-order chemical variations along ridge axes result from coupled compositional–thermal variations in the underlying mantle source.

2. Blob model of convection

Terrestrial convection models must satisfy both the geophysical constraints that require whole-mantle convection and the geochemical requirement for a reservoir isolated for a long time from the convecting mantle. In one solution [25], convecting cells of undepleted mantle are separated by intervening zones of depleted material. As an alternative to purely convective models, Becker et al. [24] suggested that large (500–800 km radius) primitive conductive blobs can survive in convecting depleted lower mantle, provided that they reside far from each other in the cores of the convective cells. This model is supported by the calculations indicating that high-viscosity blobs can survive for geologically long times in a convective medium without being absorbed [23]. The mixing efficiency is proportional to $(1+\lambda)^{-2}$ (with $\lambda = \eta_{blob}/\eta_{mantle}$ where η is the viscosity) [23,26], suggesting that these blobs

Table 1
Concentrations of heat-producing elements in MORB and Earth reservoirs

	U (ppm)	Th (ppm)	K (ppm)	H (pW/kg)	H/H^{BSE}	Ref.
MORB						
Depleted[a]	0.03	0.06	400			[50]
Transitional[b]	0.13	0.40	1600			[50]
Enriched[c]	0.55	2.00	5800			[50]
Mantle reservoirs						
Bulk silicate Earth	0.0203	0.0795	240	4.9	1	[29]
Depleted mantle	0.0030	0.0060	40	0.6	0.12	[28]
Enriched mantle[d]	0.0393	0.1430	414	9	1.8	This study
Bulk Earth	0.0144	0.0513	171	3.4	0.68	[30]

Concentrations in MORB. Compositions were selected from the Petrological Database of the Ocean Floor [50] in order to avoid both magma chamber crystallization and surface alteration effects. This has been done by considering only fresh glasses with MgO $>8\%$.

[a] Average composition of most depleted MORB is used.

[b] Composition commonly observed along chemical gradients.

[c] Enriched MORB compositions were selected in order to be representative of ridge sections whose physical characteristics (such as bathymetry) suggest that they overlie hot mantle domains.

[d] Values for enriched mantle are calculated assuming: (1) an enriched reservoir filling 30% of the mantle [32]. This imposes $H^{EM} = 9$ pW/kg (see text); (2) Th/U = 3.636 and K/U = 10545 (enriched MORB values).

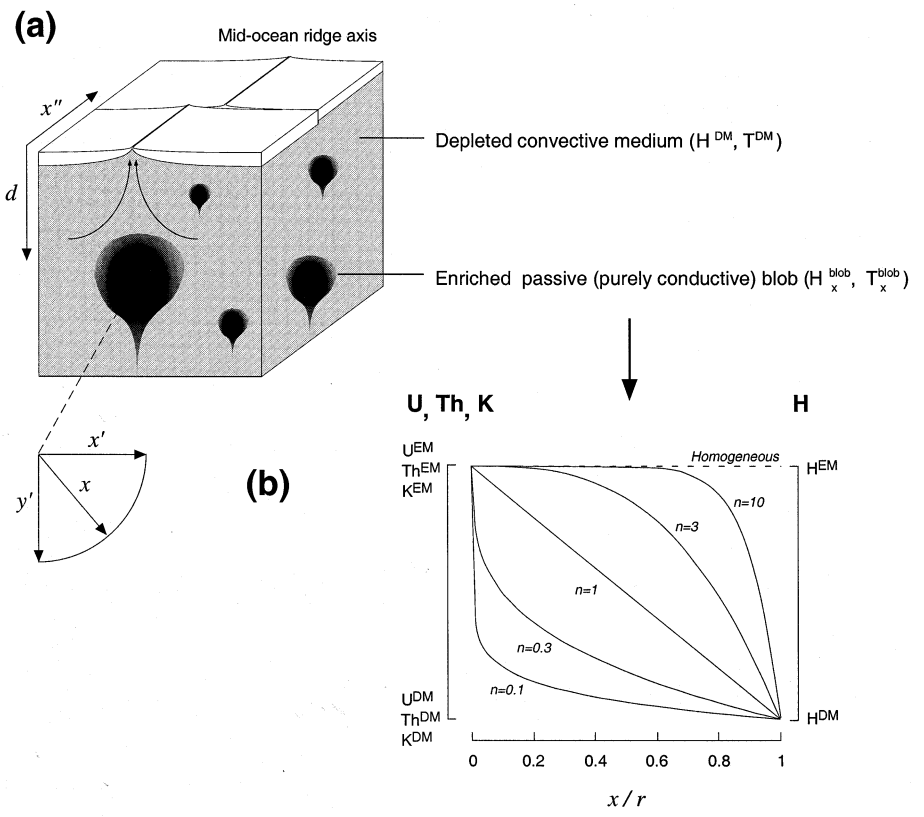

Fig. 2. Enriched passive (purely conductive) blobs in a depleted convective medium. (a) Conductive blobs should not be too close to each other to allow heat to be transported mainly by convection. Due to the high concentration of heat-producing elements, the blobs develop an excess of temperature relative to the depleted medium. The boundary condition is that the outer surface of the blob is kept at the temperature of the depleted medium (T^{DM}). x'' and d are along-axis and depth coordinates of the blob, respectively. Within blob, Polar (x) and Cartesian (x',y') coordinates systems are used. (b) Different distribution patterns of heat-producing elements in the blob are considered. r is the radius of the blob, x the distance to the center. Dashed line is for homogeneous blob. Plain line is for blob with chemical gradient (values denoted n are relative to Eq. 5). U, Th, K concentrations and derived heat production decrease from the center towards the periphery (superscripts EM and DM are for enriched and depleted material respectively). From heat generation values corrected for the loss of neutrino energy by β^- emitters [27], the relationship between heat production (H in pW/kg) and heat-producing elements concentrations (in ppm) writes: $H=(98.1\ U+26.38\ Th+0.00345\ K)\times 10^{-12}$.

may remain unmixed for a time larger than predicted in earlier models. A condition for the persistence of blobs is that their intrinsic viscosity counterbalances the viscosity decrease resulting from the excess temperature.

In the absence of a large density contrast at the 670-km discontinuity, highly viscous material from the lower mantle can ascend into the upper mantle. The viscosity of the surrounding mantle has opposing effects on the blobs. If the blobs are highly viscous, a decrease in the viscosity of the surrounding mantle: (1) increases λ and decreases the mixing efficiency; (2) increases the stirring efficiency and reduces the size of the blobs. However, if the commonly observed variations in chemical compositions along ridges [17] are due to the presence of blobs, it is evident that the blobs must survive the mixing process and must be sampled during the formation of MORB. If Becker et al. [24] are correct when they argue

that blobs are under-represented in the mantle beneath the ridges because of their intrinsically high density, another factor must counterbalance their high density.

As a framework for our model, we consider enriched conductive blobs included within a depleted convective medium beneath a spreading system (Fig. 2a). A boundary condition when solving heat-diffusion equations requires that the outer surface of the sphere be kept at the temperature of the medium (T^{DM}). This assumption has been shown to be valid as long as the time scale of convection remains significantly shorter than that of conduction [24], a condition that is fulfilled in the lower mantle [24]. The thermal Peclet number, Pe_t, which measures the relative importance of convective to conductive heat transport, is defined as:

$$Pe_t = \frac{u_0 r}{\kappa} \quad (1)$$

where u_0 is the convective medium velocity, κ is the thermal diffusivity, and r is the sphere radius. Using the characteristics of the upper mantle (Table 2) and a radius of 35–350 km, we get $50 \leq Pe_t \leq 500$, indicating that for this range of radii, the heat is transported mainly by convection. This validates the blob model for the upper mantle. However, as pointed out by Becker et al. [24], when heat is transported mainly by convection, the blobs must not be too close together. These authors proposed that the minimum half-distance between blobs is given by the characteristic diffusion length (L) which is defined by:

$$L \geq r(Pe_t)^{-1/3} \quad (2)$$

The upper mantle parameters impose $10 \leq L \leq 44$ km for $35 \leq r \leq 350$ km.

3. Heat production values

The heat production rates of mantle reservoirs decrease continuously through time (by a factor $\sim$2 during the last 2.5 Ga [27]) and depend on the initial contents of heat-producing elements. For convenience, we use here present-day estimates (see values given in Table 1) but note that rates were higher in the past. The present-day concentrations of heat-producing elements estimated in the depleted portion of the mantle [28] yield a heat production (H^{DM}) of 0.6 pW/kg. Heat production in the enriched reservoir (H^{EM}) is poorly known but can be estimated using indirect methods. From values estimated for bulk silicate Earth [29], the heat production of primitive mantle is 20.5 TW. Note that an identical value is obtained from an estimate for the entire Earth [30] if there are no heat-producing elements in the core. If the crustal contribution is 6.9 TW [31], a heat production of 13.6 TW is derived for the present-day differentiated mantle. Since the heat production of the whole mantle and H^{DM} are known, H^{EM} depends on the proportion of the mantle that is enriched. Using the minimum half-distance between blobs imposed by Pe_t, Becker et al. [24] showed that blobs (whatever their composition) have to fill 30–65% of

Table 2
Physical parameters of the upper mantle used in this study

Parameters	Value	Ref.
Heat capacity	$C_p = 1260$ J kg^{-1} K^{-1}	[53], p. 459
Thermal conductivity	$k = 4.9$ W m^{-1} K^{-1}	[53], p. 459
Mean density	$\rho = 3516$ kg m^{-3}	[53], p. 455
Acceleration of gravity	$g = 10$ m s^{-2}	[53], p. 455
Characteristic velocity of convection	$u_0 = 5$ cm yr^{-1}	[37], pp. 285–286
Blob radius	$35 \leq r \leq 350$ km	
Derived values		
Thermal diffusivity	$\kappa = 1.11 \times 10^{-6}$ m^2 s^{-1}	$k/(C_p\rho)$
Thermal Peclet number	$50 \leq Pe_t \leq 500$	Eq. 1
Characteristic half-distance between blobs	$10 \leq L \leq 44$ km	Eq. 2

the mantle. This range depends little on blob size. If enriched blobs fill 65% of the mantle (a volume equivalent to the lower mantle), we find $H^{EM} = 4.4$ pW/kg. If enriched blobs fill 30% of the mantle (a volume equivalent to that of the mantle between 1600 km and the core–mantle boundary [32]), then $H^{EM} = 9$ pW/kg. Based on the arguments discussed by Kellog et al. [32] and the evidence that enriched MORB (see Table 1) are derived from a mantle reservoir enriched relative to bulk silicate Earth, we will use the high value of H^{EM}. Note however that these estimates are bulk values relative to two main mantle reservoirs and do not exclude the existence of domains with heat productions out of this range. For example, recycling of oceanic [33] and continental [34] crust into the mantle will introduce material rich in heat-producing elements.

4. Distribution of temperature

Galer and O'Nions [35] suggested that the upper mantle is in chemical steady-state. This means that the differentiation that generates chemical heterogeneities is counterbalanced by convection which stirs and mixes the mantle domains [36]. Gurnis [22] estimated that the decay time of blobs is on the order of billions of years, a result consistent with isotopic data. The steady-state assumption regarding heat diffusion within blobs requires that the time scale of heat diffusion is shorter than the time scale of blob decay and the decrease in heat production. This assumption was shown to be reasonable by Becker et al. [24]. Using the full solution of the heat diffusion equation for an internally heated sphere, they estimated that $0.7\Delta T_{max}$ and $0.93\Delta T_{max}$ are reached after 1 and 2 Ga, respectively. The assumption of steady-state heat diffusion leads to an estimate of the temperature excess within the blobs which is greater than that predicted using a time-dependent equation. To take into account the decrease in the rate of heat production through time has the opposite effect. Further work is neededto evaluate the relative importance of these effects.

The steady-state distribution of temperature within an internally heated sphere is governed by the Fourier's law [37]:

$$k\left(\frac{d^2T}{dx^2} + \frac{2}{x}\frac{dT}{dx}\right) + \rho H = 0 \quad (3)$$

where H is the heat production per unit weight, ρ the density, k the thermal conductivity, and x the distance to the center of the sphere. The distribution of temperature in an enriched sphere of radius (r) with a uniform rate of internal heat production (H^{EM}) is [37]:

$$T_x^{blob} = T^{DM} + \frac{\rho H^{EM}}{6k}(r^2 - x^2) \quad (4)$$

where T^{DM} is the temperature of the depleted medium. The temperature is at a maximum at the center of the sphere and decreases towards the surface. The temperature gradient $|dT/dx|$ increases linearly towards the surface and is greatest at the periphery; this suggests that, in the case of departure from the purely conductive regime, convection and mixing will occur preferentially within the outer shell of the sphere. The effect will be greatest in large spheres ($r > 200$ km) for which the critical Raleigh number (Ra_C of $O(10^3)$) may be reached, allowing the spheres to convect internally. Spheres with a chemical gradient from an enriched center to a depleted periphery could form from homogeneous spheres whose external shells have mixed through time with the surrounding depleted material. In the absence of constraints on compositional variations within the blobs, we use the following general equation to express the distribution of heat production along a radial axis:

$$H_x^{blob} = (H^{DM} - H^{EM})\left(\frac{x^n}{r}\right) + H^{EM} \quad (5)$$

where H^{EM} and H^{DM} are the heat production rates of the enriched and depleted materials, respectively. Values of n ranging from 0.1 to 10 produce a sufficiently wide range of distribution patterns (Fig. 2b). Substituting Eq. 5 in Eq. 3, and twice integrating with constants of integration satisfying the boundary conditions, we obtain:

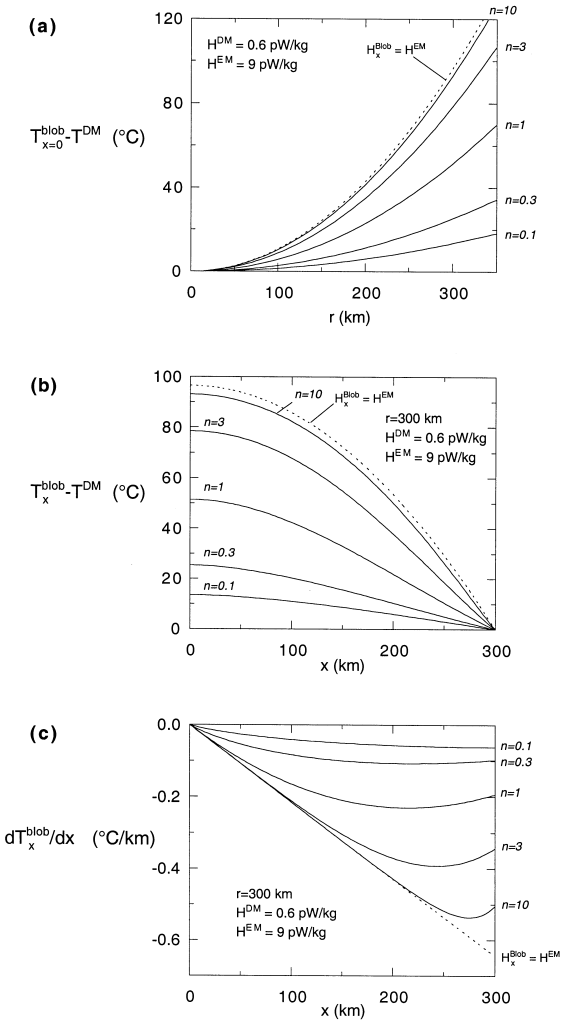

Fig. 3. Thermal distribution into the blob. (a) Temperature excess in the center of blob as a function of blob radius. Temperature is obtained from Eqs. 4 and 6 setting $x=0$. (b) Distribution of temperature within blob. Temperature is obtained from Eqs. 4 and 6 setting $r=300$ km. (c) Derived distribution of temperature gradient. (a–c) Dashed line for homogeneous blob with $H^{EM}=9$ pW/kg. For blob with chemical gradient (plain line), n values refer to the distribution of heat-producing elements within blob (see Eq. 5 and Fig. 2b), $H^{DM}=0.6$ pW/kg and $H^{EM}=9$ pW/kg.

$$T_x^{blob} = T^{DM} + \frac{\rho(H^{DM}-H^{EM})(r^{n+2}-x^{n+2})}{(n+2)(n+3)kr^n} + \frac{\rho H^{EM}}{6k}(r^2-x^2) \quad (6)$$

The temperature is that at which the solidus is intersected. In Eqs. 4 and 6 we impose $T^{DM}=1224$°C, a temperature appropriate for the formation of depleted MORB. This is the temperature required for depleted mantle to undergo 10% of melting when it ascends to the surface (see later, Eq. 9). In Fig. 3a, temperature excess in the center of the blob, relative to the surrounding mantle, is plotted versus blob radius for different distributions of heat-producing elements ($n=0.1$–10), $H^{DM}=0.6$ pW/kg, and $H^{EM}=9$ pW/kg ($\approx 15\times$ H^{DM} or $1.8\times$ H^{BSE}). Only large blobs develop significant temperature excesses and only these will be considered further. Temperature distributions and derived temperature gradients are illustrated in Fig. 3b,c for a radius of 300 km. The gradient $|dT/dx|$ is the highest for the homogeneous blob and decreases with n. The maximal thermal stability is theoretically reached when $|dT/dx|$ is both minimal and constant along the radial axis. Based on Eq. 3, this condition requires $H_x^{blob}=f(1/x)$; it can never be reached in reality because it requires an infinite concentration of heat-producing elements in the center of the blob. Nevertheless, blobs could be considered as passive and stable as long as $Ra < Ra_c$.

5. Blob melting

Before calculating the range of composition of liquids produced by blob melting, it is necessary to evaluate the influence of internal heat production in the blobs on the melting process.

5.1. Melting of a thermally heterogeneous blob

Melting occurs when the adiabat crosses the mantle solidus. During the upward migration of a blob beneath a spreading ridge, the different shells that make up the blob melt at different depths, as a function of their temperature. In a small blob, temperature differences are small; the center and periphery follow very similar adiabat paths and cross the solidus at similar depths. For a large blob, the center is much hotter than the periphery and it crosses the solidus at a greater depth. The effect increases as the rate of heat

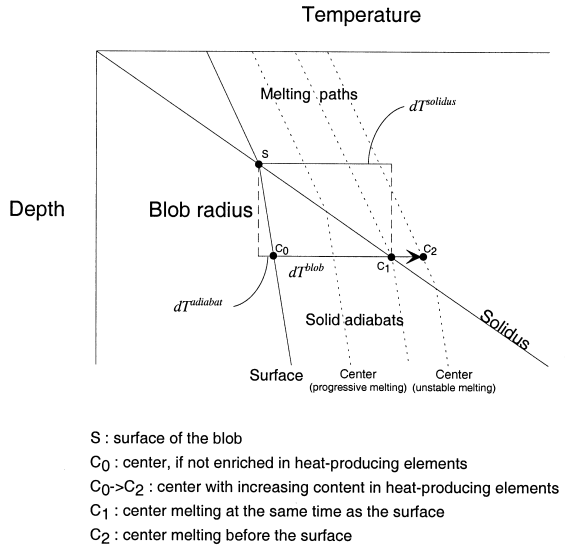

Fig. 4. Schematic depth (z) vs. temperature (T) diagram. Sub-solidus and melting paths are shown for the center (dashed lines) and the surface (plain lines) of a blob. When the surface of the blob crosses the solidus it has the (z,T) characteristics illustrated by point S. At the same time, the center of the blob is located deeper in the mantle. If the blob were not enriched in heat-producing elements, its center would lie on the same adiabat path as the surface (point C_0). Considering the adiabatic gradient ($\sim$0.6°C/km) [38], it would be only slightly hotter and would not melt since the adiabatic gradient is smaller than the solidus slope ($\sim$4.23°C/km) [39]. The effect of heat-producing elements is to increase the temperature in the center of the blob (the surface temperature remaining constant), and to move C_0 towards C_1 (illustrated by the arrow). If the content in heat-producing elements is high enough, the center of the blob could melt at the same time as its surface (C_1) or even before (C_2) if the content in heat-producing elements exceeds a threshold value.

production increases. The center of a large blob may even melt before the external part, resulting in a very unstable situation that leaves the blob highly deformed.

As illustrated in Fig. 4, progressive melting of the blob – e.g. from top to bottom – requires that the maximum temperature gradient in the blob is less than the solidus slope. This maximal gradient occurs where radial and adiabatic gradients in the blob are superimposed. This is the case along a vertical line linking the top and the center of the blob. Therefore, progressive melting requires:

$$\left|\frac{\mathrm{d}T}{\mathrm{d}x}\right|^{\mathrm{blob}} + \left|\frac{\mathrm{d}T}{\mathrm{d}z}\right|^{\mathrm{adiabat}} < \left|\frac{\mathrm{d}T}{\mathrm{d}z}\right|^{\mathrm{solidus}} \quad (7)$$

This condition is examined in the case of homogeneous blobs, which produce the highest temperature gradients (Fig. 3c). Taking 0.6°C/km for the adiabatic gradient and 4.23°C/km for the solidus slope [38,39], this condition is fulfilled for $H^{\mathrm{EM}} < 40$ pW/kg and $x < 350$ km (Fig. 5), indicating that blob melting is progressive in all reasonable cases.

5.2. Heat production and melting path

The heat required for melting (the heat of fusion, H_{f}) must be provided from within the blob itself, which is isolated from its surroundings. This results in a temperature drop and explains why the melting path has a steeper P–T slope than the solid adiabat (see Fig. 4). H_{f}, the amount of energy required for 100% melting, is about 5.10^5 J/kg [39]. This value should be compared to the radioactive heat produced during melting. In our

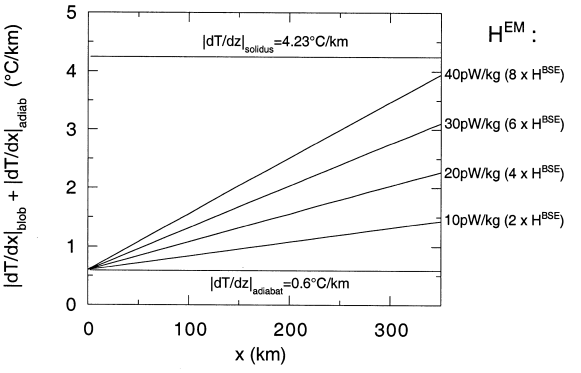

Fig. 5. Maximal gradient of temperature ($|\mathrm{d}T/\mathrm{d}x|^{\mathrm{blob}}+|\mathrm{d}T/\mathrm{d}z|^{\mathrm{adiabat}}$) for a homogeneous blob plotted versus distance to blob center (x). The maximal gradient occurs where the blob radial gradient has the same direction as the adiabat gradient, in which case they superimpose totally. This happens between the top and the center of the blob. $(\mathrm{d}T/\mathrm{d}x)^{\mathrm{blob}} = (\rho H^{\mathrm{EM}}/3k)x$ from Eq. 4, $(\mathrm{d}T/\mathrm{d}z)^{\mathrm{adiabat}} = 0.6$°C/km from [38], $(\mathrm{d}T/\mathrm{d}z)^{\mathrm{solidus}} = [(\mathrm{d}T/\mathrm{d}P)/(\mathrm{d}z/\mathrm{d}P)]^{\mathrm{solidus}} = 4.23$°C/km where $(\mathrm{d}T/\mathrm{d}P) = 12.7$°C/kb from Eq. 8 and $(\mathrm{d}z/\mathrm{d}P) = 3$ km/kb from mantle density (see Table 2). For $H^{\mathrm{EM}} < 40$ pW/kg and $x < 350$ km, $|\mathrm{d}T/\mathrm{d}x|^{\mathrm{blob}}+|\mathrm{d}T/\mathrm{d}z|^{\mathrm{adiabat}} < |\mathrm{d}T/\mathrm{d}z|^{\mathrm{solidus}}$ indicating that melting of the blob is progressive.

calculations, we will consider material with the composition of bulk silicate Earth [29] (with a heat production rate of 4.9 pW/kg), that crosses the solidus at a depth of 30 km and ascends at 5 cm/yr. This material needs 0.6 Ma to ascend from the solidus depth to the surface and during this time it produces 95 J/kg. During the melting, the heat contribution from the solid decreases while that from the liquid increases, but the global heat production of the ascending parcel of mantle is conserved. This value represents $\sim H_f/5000$ and can account for only about 0.02% of melting. It is negligible compared to the extent of melting that the material undergoes because of pressure release ($\sim$12% in our example). We can conclude, therefore, that heat production does not control the melting path and that enriched and depleted materials undergo similar amounts of melting per unit of pressure release.

6. Liquid compositions

The temperature of melting of mantle material (T_S in °C) is linked to the pressure at which the solidus is intersected (P_S in kb) by the equation [39]:

$$T_S = 1118 + 12.7P_S \quad (8)$$

Mantle temperature can also be expressed as a function of the extent of melting if it is assumed that variation in the degree of melting results wholly from differences in the pressures at the solidus. Although surface cooling slightly influences the final pressure of melting along mid-ocean ridges [40], the length of the melting column is dominantly controlled by the variations of mantle temperature. Since the temperature at the solidus directly controls the extent of melting (F), Eq. 8 can be rewritten:

$$T_S = 1118 + \alpha F \quad (9)$$

with

$$\alpha = \left(\frac{dT}{dP}\right) \Big/ \left(\frac{dF}{dP}\right)$$

where (dT/dP) is the solidus slope and (dF/dP) the amount of liquid produced per unit of pressure release. This last parameter is important in defining the melting path. It depends on heat capacity (C_p) and heat of fusion (H_f) [39] but, as previously shown, does not vary significantly with internal heat production. Taking $dF/dP = 0.012$ melt fraction/kb [18,39], we obtain $\alpha = 1058.3$°C/melt fraction.

Because U, Th and K are among to the most incompatible elements, they mainly stay in the liquid during low-pressure crystal fractionation. Liquid and source concentrations can be simply and reliably linked using melting equations. Despite its simplicity, the standard batch melting equation [41] (Eq. 10) has been shown to be adequate to model the melting process [42–44] and is used here.

$$[i]_l = \frac{[i]_s}{(D_i + F(1-D_i))} \quad (10)$$

where $[i]_l$ is the concentration of element i in the liquid, $[i]_s$ its concentration in the source, D_i the bulk mineral-melt partition coefficient. The compositions of liquids produced by melting in large ($r = 300$ km) internally heated blobs are shown in Fig. 6. The distribution of heat-producing elements in the liquid is similar to that of the source (Fig. 2b) if $n < 1$ because the temperature excess remains small and the pattern of mantle heterogeneity is unaltered by near-uniform melting. When $n > 1$, the liquid distribution is modified because large temperature excesses develop. These effects decrease with decreasing blob size and values of H^{EM} (not shown).

7. Source versus melting effects

It is generally considered that both source composition and melting processes control MORB chemical variations. Although source and melting effects are normally considered to be unrelated, the mere existence of heat-producing elements demonstrates that this cannot be true. Moreover, the geochemical behavior of these elements, which are among the most incompatible, indicates that

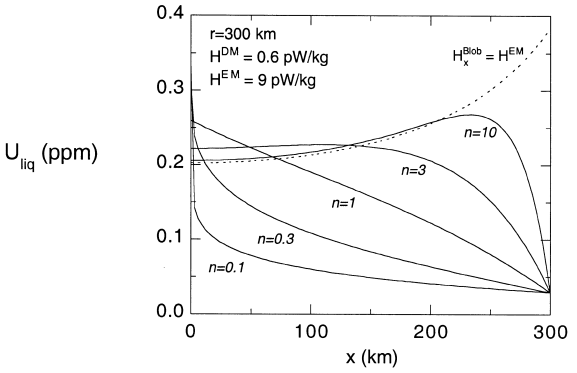

Fig. 6. Concentration of U in liquids produced by partial melting of blob. Different types of heat-producing elements distribution in blobs are considered (see Fig. 2b). Dashed line for homogeneous blob with $U^{EM} = 0.0393$ ppm and $H^{EM} = 9$ pW/kg. For blob with chemical gradient (plain lines), U concentration and heat production decrease from 0.0393 ppm/9 pW/kg in the center to 0.003 ppm/0.6 pW/kg at the surface. The temperature distribution (shown in Fig. 3b) is inferred from Eqs. 4 and 6 setting $T^{DM} = 1224$°C (temperature at which the depleted mantle crosses the solidus in order to undergo 10% of melting, from Eq. 9). The extent of melting is derived from the temperature using Eq. 9, and is combined with the batch melting equation (Eq. 10) to infer liquid concentrations. The solid–liquid partition coefficient used is $D_U = 0.0026$ [15]. A radius of 300 km is considered and the concentrations are reported along the blob radial axis.

the degree of mantle enrichment and the extent of partial melting should be positively correlated. On the other hand, the two parameters have competing effects on MORB compositions. This is because mantle enrichment increases concentrations in MORB whereas a greater extent of melting has the opposite effect. The blob model offers the opportunity to evaluate the relative contributions of the two parameters. This is done by calculating the composition of liquids produced by melting in blobs of variable size and concentrations of U, Th and K. The competition between source composition and the extent of melting is extreme at the center of homogeneous blobs because this is where the greatest temperature excesses are produced (Fig. 3a,b) and where the highest depletion occurs during the melting event. In Fig. 7, the U contents in liquids derived from melting in blob centers are plotted against blob enrichment. For small blobs ($r < 100$ km), the extent of melting does not vary much in response to source enrichment and a close-to-linear relationship exists between source and liquid compositions. For larger blobs, the extent of melting increases with source enrichment and the blob radius; liquid compositions are depleted relative to the linear law. It is important to note that, in all cases, source and liquid concentrations are positively correlated. Even in less favorable cases, for blobs with the biggest radii, U concentrations in the liquids increase slightly with source enrichment despite a drastic increase in the extent of melting. Considering now the outermost shell of the blob, its temperature and extent of melting are insensitive to blob composition and identical to that of the depleted medium. Therefore, the more enriched the blob, the more enriched the liquids produced by melting in the outermost shell. In summary, despite the complications that arise from melting processes, liquid compositions reflect source compositions.

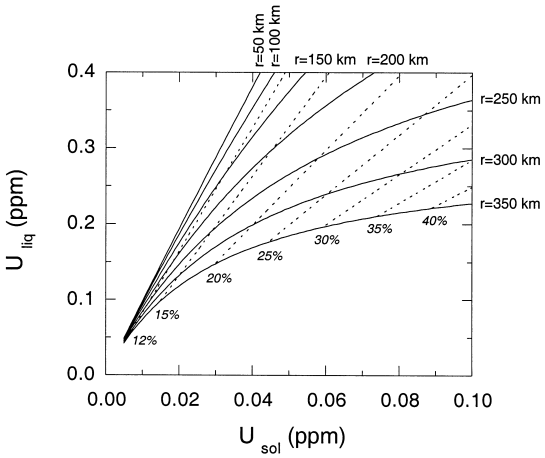

Fig. 7. U content in liquids produced by melting the center of homogeneous blob plotted versus enrichment in U. Heat production is inferred from U concentration using Th/U = 3.92 and K/U = 11823 (bulk silicate Earth values [29]), and temperature from Eq. 4 settings $x = 0$ and $T^{DM} = 1224$°C (temperature at which the depleted mantle crosses the solidus in order to undergo 10% of melting, from Eq. 9). Extent of melting is derived from temperature using Eq. 9, and is combined with the batch melting equation (Eq. 10) to infer liquid concentrations. The solid–liquid partition coefficient used is $D_U = 0.0026$ [15].

8. Along-axis thermal and chemical variations

Blobs trapped in upwelling mantle could be the cause of thermal and chemical anomalies along mid-ocean ridges. The 'digestion' of such blobs at a spreading center is a complex process that involves different physical laws to describe their progressive deformation and destruction. To model the process would require extensive calculations. In this section we conduct a preliminary analysis by considering ridge-centered, non-deformable ascending blobs that reach and pass through the solidus. We estimate the along-ridge thermal and chemical anomalies resulting from this process.

This approach requires a Cartesian coordinate system (x',y') that is defined by:

$$x = (x'^2 + y'^2)^{\frac{1}{2}} \quad (11)$$

where $x' = x''-r$ and $y' = z-d$ (see Fig. 2a). x'' is the distance along the ridge axis, z is the solidus depth and d the depth to the center of the blob (all in meters). From mantle density (Table 2), the solidus equation (Eq. 8) can be rewritten:

$$T_S = 1118 + 0.00423z \quad (12)$$

For homogeneous blobs, Eqs. 4, 11 and 12 yield a second-degree equation which, once x'' and d are given, is solved analytically for z. For heterogeneous blobs, Eqs. 6, 11 and 12 are solved using numerical methods. From Eq. 5, the distribution of U, Th and K in heterogeneous blobs at solidus depth is given by:

$$[i]^{\text{blob}}_{S,x'',z} = \frac{([i]^{DM}_S - [i]^{EM}_S)}{r^n} \cdot ((x''-r)^2 - (z-d)^2)^{\frac{n}{2}} + [i]^{EM}_S \quad (13)$$

The composition of lava erupting at the surface is a complicated weighted average of liquids produced at depth. Nonetheless, as mentioned above, the standard equilibrium melting equation [41] (Eq. 10) adequately models the melting process [42–44] and is used here. The second problem we have to face is that, at a given location, the temperature and composition of material crossing the solidus, and the composition of the liquids that form, change continuously. Rather than estimating with few constraints how the different liquids mix in the melting column, we calculate individual batch melts, and argue that the chemical variations in MORB reflect the instantaneous variations of liquids produced at depth. Indeed, although a consequence of mixing liquids in the melting column is to buffer the chemical anomaly, the overall pattern should be conserved. Along-axis thermal and chemical anomalies formed when large blobs ($r = 300$ km) cross the solidus are shown in Fig. 8. When the center of the blob is at a depth of 300 km, only its upper part is in the melting zone. The resulting thermal anomaly is small and the chemical anomaly is of high amplitude only for homogeneous and near-homogeneous ($n = 10$) blobs. As the blob ascends, it progressively crosses the solidus and this results in an increase in the size of the along-axis thermal and chemical anomalies. The material reaching the melting zone becomes hotter, causing it to melt at deeper depth and to undergo a higher degree of melting. The result is an increase of the thermal anomaly (Fig. 8a), while the chemical anomalies evolve differently in response to the combination of thermal and compositional effects (Fig. 8b). At a depth of 50 km, the center of the residual blob is in the melting zone (half of the blob has already undergone partial melting) and the thermal anomaly is at a maximum. The chemical anomaly displays very different patterns depending on the distribution of heat-producing elements in the mantle source. During the entire process, most enriched liquids are produced at the margins of the anomaly for homogeneous blobs, whereas they coincide with the center of the anomaly for blobs with significant chemical gradient ($n < 3$).

9. Discussion and conclusion

The blob model indicates that the relations between melting processes and source compositions are controlled mainly by blob size. Because small blobs ($r < 100$ km) develop only minor temperature excesses, even if the mantle is extremely heterogeneous on a small scale, it will maintain a

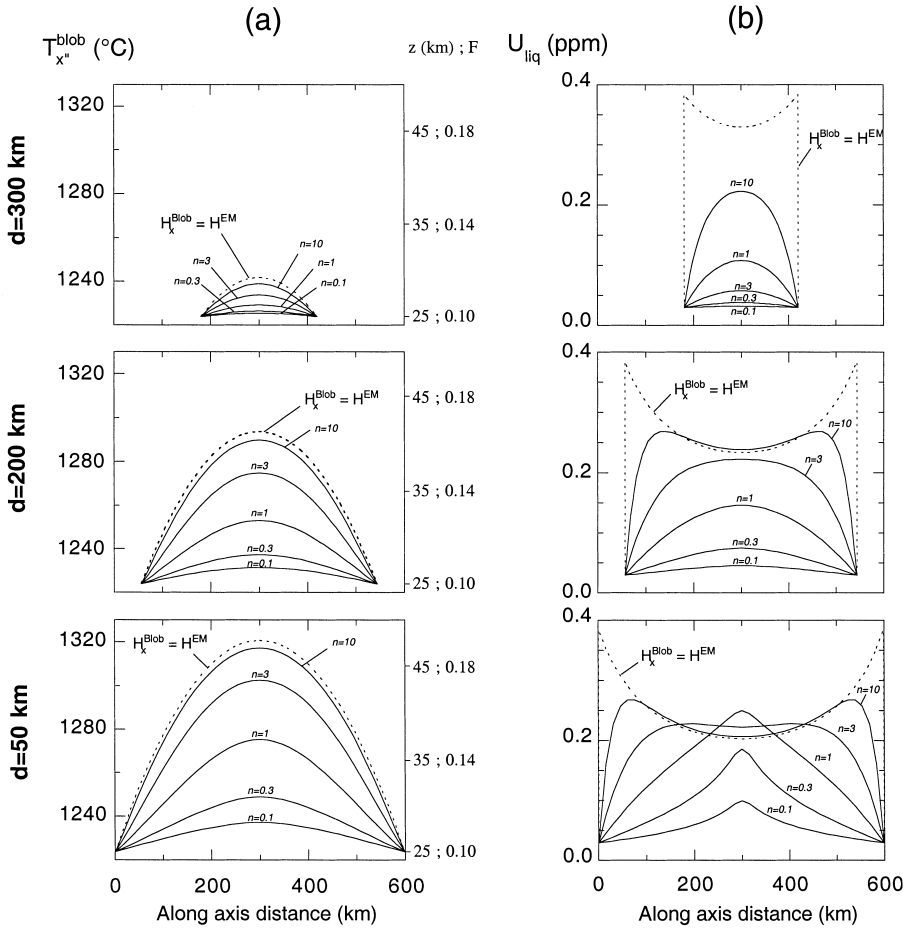

Fig. 8. Along-axis thermal and chemical anomalies at solidus depth resulting from the upwards migration of large blob ($r = 300$ km). Ridge-centered, non-deformable blob is considered at different depths (d being the depth of blob center). Dashed line is for homogeneous blob with $H^{EM} = 9$ pW/kg ($U^{EM} = 0.0393$ ppm). Plain line is for blob with chemical gradient with $H^{DM} = 0.6$ pW/kg ($U^{DM} = 0.003$ ppm) and $H^{EM} = 9$ pW/kg ($U^{EM} = 0.0393$ ppm). n values refer to the distribution of heat-producing elements within blob (see Eq. 5; and Fig. 2b). (a) Thermal anomaly. Depth of solidus intersection (z) and extent of melting (F) are also indicated. z is obtained as explained in text and is used to calculate the temperature using Eq. 12. F is then obtained from Eq. 9. (b) Chemical anomaly. Composition of liquids is obtained as explained in Fig. 6 caption. (a,b) At a depth of 300 km, only the upper part of the blob is in the melting layer. The thermal anomaly is small for all types of blob. However, the chemical anomaly is already of high amplitude for homogeneous or nearly homogeneous blob ($n = 10$). As the blob ascents, the thermal anomaly increases but conserves the same shape, while the pattern of chemical anomaly evolves differently depending on the distribution of heat-producing elements in the melting region. At a depth of 50 km, the center of the blob is in the melting zone and the thermal anomaly is at a maximum.

nearly uniform temperature. The presence of small blobs may explain isolated chemical 'spikes' along mid-ocean ridges, but they do not influence the melting process. Large ($r \sim 300$ km), uniformly enriched blobs develop significant temperature excesses ($\Delta T \sim 100$°C). Within such blobs, the temperature gradient increases linearly from the center towards the margin where the material is in contact with the convecting depleted mantle. In the case of departure from the purely conductive regime, the outermost shell of the blob mixes with the surrounding mantle. The resultant chemically zoned blobs develop significantly smaller temperature excesses than the homogeneous blobs

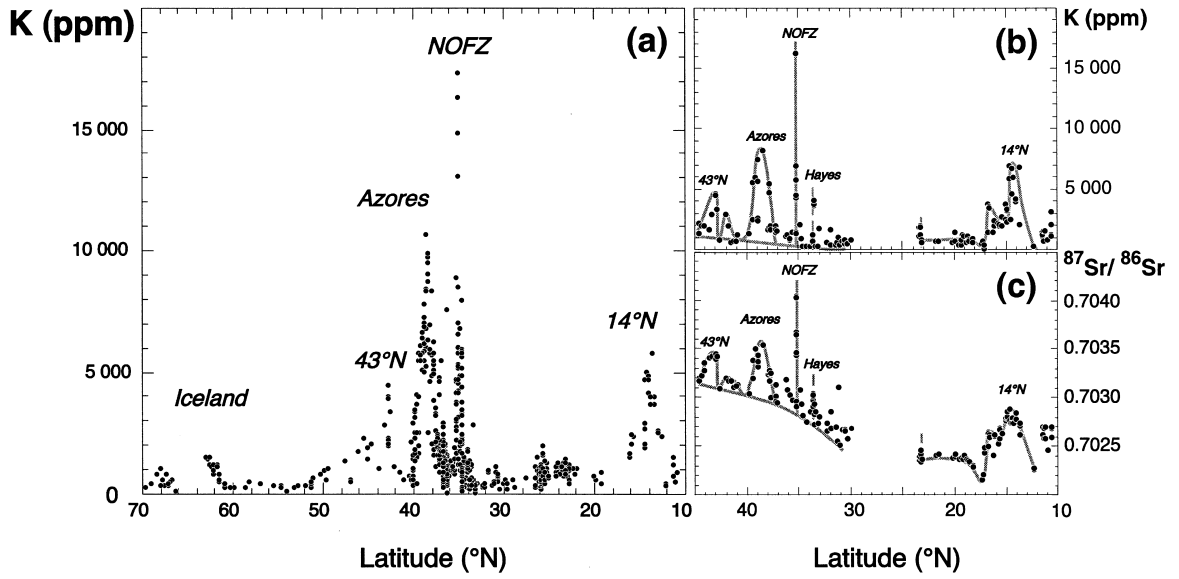

Fig. 9. K concentration and $^{87}Sr/^{86}Sr$ along the North Mid-Atlantic Ridge. (a) Published K data on basaltic glasses are taken from the Petrological Database of the Ocean Floor of the LDEO [50] and plotted along the Mid-Atlantic Ridge from 10 to 70°N. We choose to show K distribution because of the large number of data available (compared to U and Th). Given that the compatibilities of U and Th are similar to that of K, these elements should show similar patterns. Along the ridge, K concentrations display first-order variations with different wavelengths and amplitudes. Short-wavelength anomalies of high amplitude are observed North of the Oceanographer Fracture Zone (NOFZ) or in the vicinity of the Azores. Such signals can be explained by melting enriched blobs that are sufficiently small to develop only minor temperature excess. Long-wavelength anomalies of moderate amplitude are seen near 45°N or in the vicinity of Iceland. They are attributed to the extensive melting of large and enriched blobs with high temperature excess in their centers. An intermediate case is observed at 14°N. The wavelengths of the anomalies, as well as their amplitudes, also depend on the depths of blobs beneath the spreading axis (Fig. 8). The asymmetric nature of an anomaly (i.e. 14°N) can be accounted for by an enriched mantle blob located off-axis. Thus, the observed chemical variations may also reflect different types of blob–ridge interaction. Composite signals are seen where spikes are superimposed to signals of longer wavelength (43°N, 14°N). Such signals may reflect a situation in which small blobs are included in larger ones, or a more complex distribution of blobs in the mantle source. (b,c) K concentrations and $^{87}Sr/^{86}Sr$ ratios are shown along the Mid-Atlantic Ridge from 10 to 45°N. K and $^{87}Sr/^{86}Sr$ analyses were performed on the same samples in the same lab (CNRS-IFREMER/Brest) ([47,51,52]; and unpublished data). K and $^{87}Sr/^{86}Sr$ display coherent first-order variations along the ridge. A systematic increase in the $^{87}Sr/^{86}Sr$ baseline – defined as the locus of the minima – is observed between 30 and 45°N. A similar feature, although less pronounced, is also seen in K variation. This reinforces the observation that K and $^{87}Sr/^{86}Sr$ display coherent variations along the ridge. This observation alone demonstrates that, despite the effects of melting, the variations in incompatible element concentration observed along mid-ocean ridges mainly reflect mantle composition variations, as predicted by the model.

from which they form. Temperature gradients in zoned blobs are flatter, suggesting that they are thermally more stable. The survival of these blobs depends both on their thermal stability and on the viscosity contrast (λ), which is expected to decrease as a result of mixing.

The concentration of heat-producing elements has been combined with the derived temperature distribution to assess the composition of liquids produced during blob melting. For all the types of solid distribution that we considered, the temperature increases systematically towards the center of the blob; the distribution of heat-producing elements in liquids is variable and integrates both source and melting effects. Melting in a homogeneous blob would produce a U-shaped pattern in diagrams plotting element concentration versus distance along the ridge because less enriched liquids are produced at the hot center of the blob and more enriched liquids are produced at the margins (Fig. 8). This type of pattern is not observed along mid-ocean ridges (Fig. 9). In con-

trast, melting in blobs with significant chemical gradients ($n < 3$) can produce the commonly observed hump-shaped chemical anomaly centered on the thermal anomaly.

Thus, based on simple thermal and melting considerations, we believe that the blobs are chemically and thermally zoned. Element distributions with $1 < n < 3$ satisfy both (1) the need for a significant thermal anomaly that can explain the variation of ridge depth and, (2) the correlation between the degree of chemical enrichment in MORB and the magnitude of the thermal anomaly.

A factor that has not been considered is the role of water, which causes the mantle to start to melt at greater depth. During mantle melting, water is only slightly less incompatible than U, Th and K (similar to La and Ce, see Fig. 1) [45]. The concentrations of water and the heat-producing elements probably are coupled and have a similar influence on melting and MORB compositions. At first approximation, the influence on melting of the heat-producing elements will be enhanced by the presence of water. In detail, however, the influence of water is more complex because the viscosity increase associated with dehydration prevents dynamic upwelling beneath the spreading axis [46], and this significantly modifies along-ridge variations of MORB compositions.

In order to compare model predictions with data, we report K concentrations and $^{87}Sr/^{86}Sr$ along the North Mid-Atlantic Ridge (Fig. 9). Given that the compatibilities of U and Th are similar to that of K, these elements should show similar patterns. Two observations can be made:

1. Along the ridge, K concentrations display first-order variations with different wavelengths and amplitudes (Fig. 9a). Short-wavelength signals of high amplitude are seen North of Oceanographer Fracture Zone (NOFZ) and in the vicinity of the Azores. In contrast, long-wavelength signals of moderate amplitude characterize the Iceland and 45°N regions. An intermediate situation occurs near 14°N. According to the blob model, the wavelength depends on blob size, while the magnitude of the signal depends on the composition and temperature. However, because the temperature in the blob is a function of its size, the magnitude of the chemical anomaly will also be related, indirectly, to the size of the blob. The largest blobs develop large temperature excess, which increases the extent of melting and attenuates the amplitude of the chemical anomaly in the resultant magmas. This appreciation of the factors that relate the chemical compositions of MORB to the size and nature of blobs allows us to interpret the data illustrated in Fig. 9. For example, the high-amplitude chemical spike seen NOFZ could result from melting of a small but highly enriched blob. Because of its small size, the blob develops only a minor temperature excess and undergoes a modest extent of partial melting (similar to that of the surrounding depleted mantle). In contrast, the long-wavelength anomaly of moderate amplitude associated with Iceland could be produced by extensive melting of a large and hot blob.
2. K behaves coherently with $^{87}Sr/^{86}Sr$, a parameter that only relies on the source composition and does not change during partial melting (Fig. 9b,c). This observation validates one conclusion of our model; namely, although the contents of incompatible elements in magmas depend both on the mantle source concentration and on the extent of partial melting, the chemical signature of MORB mainly reflects that of the mantle source.

In conclusion, our model based on highly incompatible elements suggests that the first-order chemical variations in MORB result from coupled compositional–thermal variations in the underlying mantle source. It contrast with previous approaches in which chemical variations in MORB are interpreted in terms of variations of a single parameter such as mantle temperature [18] or surface cooling [40]. However, it does not contradict these models, which get around the problem of source heterogeneity by considering only regions far from large chemical anomalies [18] or by using heterogeneity-corrected parameters [40]. Despite the simplifying assumptions used in the model, the results demonstrate that the chemical–thermal relationship has to be taken into account when

interpreting the global chemical variations in MORB.*[SK]*

Acknowledgements

We thank M. Manga, L. Moresi and two anonymous reviewers for their comments on versions of this manuscript. We are grateful to S.D. King for handling the manuscript and his encouragement. We also thank A.W. Hofmann, M. Regelous and N.T. Arndt for discussions and comments on the manuscript. This work benefited from financial support from IFREMER (Brest) and Max-Planck Institut (Mainz).*[SK]*

References

[1] G.F. Davies, Thermal histories of convective Earth's models and constraints on radiogenic heat production in the Earth, J. Geophys. Res. 85 (1980) 2517–2530.
[2] G. Schubert, D. Stevenson, Whole planet cooling and the radiogenic heat sources contents of the Earth and Moon, J. Geophys. Res. 85 (1980) 2531–2538.
[3] D.L. Turcotte, On the thermal evolution of the Earth, Earth Planet. Sci. Lett. 48 (1980) 53–58.
[4] D. McKenzie, F.M. Richter, Parameterized thermal convection in a layered region and the thermal history of the Earth, J. Geophys. Res. 86 (1981) 11667–11680.
[5] M.J. Jackson, H. Pollack, On the sensitivity of parameterized convection to the rate of decay of internal heat sources, J. Geophys. Res. 89 (1984) 10103–10108.
[6] U.R. Christensen, Thermal evolution models for the Earth, J. Geophys. Res. 90 (1985) 2995–3007.
[7] D.R. Williams, V. Pan, Internally heated mantle convection and the thermal and degassing history of the Earth, J. Geophys. Res. 97 (1992) 8937–8950.
[8] T. Spohn, G. Schubert, Modes of mantle convection and the removal of heat from the Earth's interior, J. Geophys. Res. 87 (1982) 4682–4696.
[9] H. Bougault, L. Dosso, Trace element fractionation contributes to mantle convection, Terra Nova 9 (1997) 54.
[10] S. Honda, A preliminary analysis of convection in a mantle with a heterogeneous distribution of heat-producing elements, Phys. Earth Planet. Inter. 34 (1984) 68–76.
[11] S. Honda, D.A. Yuen, Mantle convection with moving heat-source anomalies: geophysical and geochemical implications, Earth Planet. Sci. Lett. 96 (1990) 349–366.
[12] U. Hansen, D.A. Yuen, Extended-Boussinesq thermal–chemical convection with moving heat sources and variable viscosity, Earth Planet. Sci. Lett. 176 (2000) 401–411.
[13] M. Ogawa, Effects of chemical fractionation of heat-producing elements on mantle evolution inferred from a numerical model of coupled magmatism-mantle convection system, Phys. Earth Planet. Int. 83 (1994) 101–127.
[14] T.Z. LaTourette, D.S. Burnett, Experimental determination of U and Th partitioning between clinopyroxene and natural and synthetic basaltic liquid, Earth Planet. Sci. Lett. 110 (1992) 227–244.
[15] C.C. Lundstrom, H.F. Shaw, F.J. Ryerson, D.L. Phinney, J.B. Gill, Q. Williams, Compositional controls on the partitioning of U, Th, Ba, Pb, Sr and Zr between clinopyroxene and haplobasaltic melts: implication for the uranium series disequilibria in basalts, Earth Planet. Sci. Lett. 128 (1994) 407–423.
[16] A. Zindler, E. Jagoutz, Mantle cryptology, Geochim. Cosmochim. Acta 52 (1988) 319–333.
[17] H. Bougault, M. Treuil, Mid-Atlantic Ridge zero-age geochemical variations between Azores and 22°N, Nature 286 (1980) 209–212.
[18] E.M. Klein, C. Langmuir, Global correlations of ocean ridge basalt chemistry with axial depth and crustal thickness, J. Geophys. Res. 92 (1987) 8089–8115.
[19] A.W. Hofmann, Chemical differentiation of the Earth: the relationship between mantle, continental crust, and oceanic crust, Earth Planet. Sci. Lett. 90 (1988) 297–314.
[20] Y. Niu, R. Batiza, An empirical method for calculating melt compositions produced beneath mid-ocean ridges: application for axis and off-axis (seamounts) melting, J. Geophys. Res. 96 (1991) 21753–21777.
[21] R.J. Kinzler, T.L. Grove, Primary magmas of mid-ocean ridge basalts. 2. Applications, J. Geophys. Res. 97 (1992) 6907–6926.
[22] M. Gurnis, Stirring and mixing in the mantle by plate-scale flow: large persistent blobs and long tendrils coexist, Geophys. Res. Lett. 13 (1986) 1474–1477.
[23] M. Manga, Mixing of heterogeneities in the mantle: effect of viscosity differences, Geophys. Res. Lett. 23 (1996) 403–406.
[24] T.W. Becker, J.B. Kellogg, R.J. O'Connell, Thermal constraints on the survival of primitive blobs in the lower mantle, Earth Planet. Sci. Lett. 171 (1999) 351–365.
[25] G. Schubert, T. Spohn, Two-layer mantle convection and the depletion of radioactive elements in the lower mantle, Geophys. Res. Lett. 8 (1981) 951–954.
[26] N. Merveilleux du Vignaux, L. Fleitout, Stretching and mixing of viscous blobs in the Earth's mantle, EOS Trans. Am. Geophys. Union 81 (2000) F1221.
[27] W.R. Van Schmus, Natural radioactivity of the crust and mantle, in: T.J. Ahrens (Ed.), Global Earth Physics – A Handbook of Physical Constants, AGU, Washington, DC, 1995, pp. 283–291.
[28] K.P. Jochum, A.W. Hofmann, E. Ito, H.M. Seufer, W.M. White, K, U and Th in mid-ocean ridge basalts glasses and heat production, K/U and K/Rb in the mantle, Nature 306 (1983) 431–436.
[29] W.F. McDonough, S.-S. Sun, The composition of the Earth, Chem. Geol. 120 (1995) 223–253.
[30] C. Allègre, G. Manhès, E. Lewin, Chemical composition

of the Earth and the volatility control on planetary genetics, Earth Planet. Sci. Lett. 185 (2001) 49–69.
[31] R.L. Rudnick, W.F. McDonough, R.J. O'Connell, Thermal structure, thickness and composition of continental lithosphere, Chem. Geol. 145 (1998) 395–411.
[32] L.H. Kellog, B. Hager, R.D. vanderHilst, Compositional stratification in the deep mantle, Science 283 (1999) 1881–1884.
[33] F. Albarède, Time-dependent models of U–Th–He and K–Ar evolution and layering of mantle convection, Chem. Geol. 145 (1998) 413–429.
[34] N. Coltice, F. Albarède, P. Gillet, ^{40}K–^{40}Ar constraints on recycling continental crust into the mantle, Science 288 (2000) 845–847.
[35] S.J.G. Galer, R.K. O'Nions, Residence time of thorium, uranium and lead in the mantle with implications for mantle convection, Nature 316 (1985) 778–782.
[36] C.J. Allègre, E. Lewin, Isotopic systems and stirring times of the Earth's mantle, Earth Planet. Sci. Lett. 136 (1995) 629–646.
[37] D. Turcotte, G. Schubert, Geodynamics-Application of Continuum Physics to Geological Problems, J. Wiley and Sons, New York, 1982, 450 pp.
[38] D. McKenzie, M.J. Bickle, The volume and composition of melt generated by extension of the lithosphere, J. Petrol. 29 (1988) 625–679.
[39] C. Langmuir, E.M. Klein, T. Plank, Petrological systematics of mid-ocean ridge basalts: constraints on melt generation beneath ocean ridges, in: J. Phipps Morgan, D.K. Blackman, J.M. Sinton (Eds.), Mantle Flow and Melt Generation at Mid-Ocean Ridges, Geophys. Monogr. Ser., Vol. 71, AGU, Washington, DC, 1992, pp. 183–280.
[40] Y. Shen, D.W. Forsyth, Geochemical constraints on initial and final depths of melting beneath mid-ocean ridges, J. Geophys. Res. 100 (1995) 2211–2237.
[41] D.M. Shaw, Trace element fractionation during anatexis, Geochim. Cosmochim. Acta 34 (1970) 237–243.
[42] C.C. Lundstrom, J. Gill, Q. Williams, M.R. Perfit, Mantle melting and basalt extraction by equilibrium porous flow, Science 270 (1995) 1958–1961.
[43] N. Ribe, The generation and composition of partials melts in the Earth's mantle, Earth Planet. Sci. Lett. 73 (1985) 361–376.
[44] M. Spiegelman, T. Elliot, Consequences of melt transport for uranium series disequilibrium in young lavas, Earth Planet. Sci. Lett. 118 (1993) 1–20.
[45] L.V. Danyushevsky, S.M. Eggins, T.J. Falloon, D.M. Christie, H_2O abundance in depleted to moderately enriched mid-ocean ridge magmas; part 1: incompatible behavior, implications for mantle storage, and origin of regional variations, J. Petrol. 41 (2000) 1329–1364.
[46] G. Ito, Y. Shen, G. Hirth, C.J. Wolfe, Mantle flow, melting, and dehydration of the Iceland mantle plume, Earth Planet. Sci. Lett. 165 (1999) 81–96.
[47] L. Dosso, H. Bougault, J.-L. Joron, Geochemical morphology of the North Mid-Atlantic Ridge, 10°–24°N: trace element-isotope complementarity, Earth Planet. Sci. Lett. 120 (1993) 443–462.
[48] I. Vlastélic, L. Dosso, H. Bougault, D. Aslanian, L. Géli, J. Etoubleau, M. Bohn, J.L. Joron, C. Bollinger, Chemical systematics of an intermediate spreading ridge: The Pacific-Antarctic Ridge between 56 and 66°S, J. Geophys. Res. 105 (2000) 2915–2936.
[49] C. Hémond, I. Vlastélic, H. Bougault, New constraints on the origin of the 14°N anomaly (Mid-Atlantic Ridge) from highly magmaphile elements, Chem. Geol. (in revision).
[50] The Petrological Database of the Ocean Floor of the LDEO (http://petdb.ldeo.columbia.edu/petdb/).
[51] L. Dosso, H. Bougault, C. Langmuir, C. Bollinger, O. Bonnier, J. Etoubleau, The age and distribution of mantle heterogeneity along the Mid-Atlantic Ridge (31–41°N), Earth Planet. Sci. Lett. 170 (1999) 269–286.
[52] L. Dosso, S. Karpenko, H. Bougault, De l'influence des points triples sur la structure géochimique de la ride médio-atlantique entre 10 et 50°N de latitude et-ou inversement, Lettre Dorsales 8/1-2 (2001) 30–34 (also at: http://www-sdt.univ-brest.fr/~jerome/ldorsales/lettre8_dosso.pdf).
[53] F.D. Stacey, Physics of the Earth, 3rd edn., Brookfield Press, Kenmore, 1992, 513 pp.